*J. Fluid Mech.* (2002), *vol.* 463, *pp.* 313–343.  
DOI: 10.1017/S0022112002008819 Printed in the United Kingdom

# Investigation of a 'transonic resonance' with convergent–divergent nozzles

By K. B. M. Q. ZAMAN[1], M. D. DAHL[1], T. J. BENCIC[1] AND C. Y. LOH[2]

[1]NASA Glenn Research Center, Lewis Field, Cleveland, OH 44135, USA
[2]Taitech Inc., 1430 Oak Court, Beavercreek, OH 45430, USA

(Received 8 February 2001 and in revised form 3 January 2002)

Experimental studies have shown that convergent–divergent nozzles, when run at low pressure ratios, often undergo a flow resonance accompanied by emission of acoustic tones. The phenomenon, different in characteristics from conventional 'screech' tones, is addressed in this paper. Unlike screech, the resonant frequency ($f_N$) increases with increasing supply pressure. There is a 'staging' behaviour; odd-harmonic stages resonate at lower pressures while the fundamental occurs in a wide range of higher pressures corresponding to a 'fully expanded Mach number' ($M_j$) around unity. Within a stage, $f_N$ varies approximately linearly with $M_j$; the slope of the variation steepens when the angle of divergence of the nozzle is decreased. Based on the data, correlation equations are provided for the prediction of $f_N$. A companion computational study captures the phenomenon and predicts the frequencies, including the stage jump, quite well. While the underlying mechanisms are not completely understood yet, it is clear that the unsteadiness of a shock occurring within the divergent section plays a direct role. The shock drives the flow downstream like a vibrating diaphragm, and resonance takes place similarly to the (no-flow) acoustic resonance of a conical section having one end closed and the other end open. Thus, the fundamental is accompanied by a standing one-quarter wave within the divergent section, the next stage by a standing three-quarter wave, and so on. The distance from the foot of the shock to the nozzle exit imposes the pertinent length scale. The principal trends in the frequency variation are explained qualitatively from the characteristic variation of that length scale. A striking feature is that tripping of the nozzle's internal boundary layer tends to suppress the resonance. It is likely that the trip effect occurs due to a break in the azimuthal coherence of the unsteady flow.

## 1. Introduction

Flow through a nozzle, especially one involving an abrupt area change, often encounters aeroacoustic resonance. Such flows through 'whistler nozzles' have been studied by Hill & Greene (1977) and by Hussain & Hasan (1983). Resonance of similar flows discharging through a duct or 'ejector', involving choked and supersonic conditions, have been studied by Witczak (1977) and by Krothapalli & Hsia (1996). The resonance in many cases could be traced to a coupling between the duct acoustic modes and the instability of the shear layer originating from the sudden expansion. With supersonic flows, screech tones (Powell 1953; Tam 1995; Raman 1998), themselves involving a not-well-understood feedback loop, could come into play and interact with the duct acoustic modes to set up a more complex resonance.

The present study concerns nozzles with a smooth convergence to the throat and then a smooth divergence up to the exit without any sudden area change. Resonance and tones are also encountered with such a nozzle. As the pressure driving the flow is gradually increased or when the flow is gradually brought to a halt from an operating condition, tones of various frequencies may be heard. Most well known are the screech tones that occur at relatively large pressures involving off-design, overexpanded or underexpanded conditions. Tones can also occur at very low pressures with entirely subsonic flow, often due to flow-induced acoustic resonance of the jet facility. In the present study the focus is on an intermediate range of pressures when a shock exists within the diverging section of the nozzle. In this range of operating conditions the flow often locks on to a resonance accompanied by very loud tones.

Such tones have been noted in convergent–divergent (C–D) nozzles by others 'as a precursor to screech' (J. M. Seiner 1998, private communication), as well as in subsonic diffusers by the authors (Zaman & Dahl 1990). In industrial tests with nozzles a howling sound has sometimes been heard at low pressure ratios. About two decades ago, a series of experiments was conducted with a two-dimensional diffuser run at 'transonic' conditions (Chen, Sajben & Kroutil 1979; Sajben, Bogar & Kroutil 1980; Bogar, Sajben & Kroutil 1983; Hsieh & Coakley 1987). A self-excited flow oscillation was observed; the results of this and some other past work will be compared in § 4.1. However, a literature search on nozzle aerodynamics and jet noise yielded no other documentation of the phenomenon. Even though the tone could be just as intense and easily mistaken as screech on a casual observation, to the authors' knowledge, there has not been any report or recognition of it in the vast literature dealing with screech. Our first investigation was conducted about two years ago (Zaman & Dahl 1999). Those results, distinguishing the phenomenon from conventional screech tones, will be summarized in § 3.1. However, full details remained far from clear and the study was continued. This was justified since, apart from academic curiosity, the phenomenon had significant practical relevance. The reader may appreciate this relevance after the following discussion of figures 1 and 2.

Variations of the tone frequency for a variety of nozzles are shown in figure 1. The jet from a given nozzle exhausted into the ambient of the test chamber. The frequency was measured by spectral analysis of a microphone signal, the tone being represented by a sharp spike in the spectra. The figure includes data from nozzles as small as $\frac{1}{4}$ in. to as large as $3\frac{1}{2}$ in. in diameter (table 1; notations are explained in § 2). There are also sets of data from a rectangular nozzle and a circular, co-annular nozzle. These data make it amply clear that the phenomenon is quite common, at least in the laboratory environment, and must be understood when considering mixing and noise of the ensuing jet. (The dotted lines in this figure represent flow regimes based on one-dimensional analysis, discussed in § 3.1.)

The phenomenon requires that the internal surface of the nozzle be clean and smooth. Figure 2 shows noise spectra for the co-annular nozzle with a convergent–divergent outer annulus (Zaman & Papamoschou 2000). The solid curve is for normal run conditions with a smooth interior; the spike at 1.63 kHz represents the resonant tone. The dashed curve is for the same operating conditions except that the boundary layer in the outer annulus is tripped. The trip almost suppresses the tone! Here, let us look at the data from a 'reversed' perspective and make the following observation. An inspection reveals that there is still some energy at the resonant frequency. In fact, it took several trials with boundary layer tripping to achieve the best suppression, as shown. This implies that in a practical nozzle, often with non-ideal surface conditions, the subject resonance may not be a problem outright but its mechanism may still be

| Nozzle | Shape | $D_t$ (in.) | $D_e$ (in.) | $L$ (in.) | $\theta$ (deg.) |
|---|---|---|---|---|---|
| 1 | Circular | 0.25 | 0.36 | 0.375 | 8.34 |
| 2 | Circular | 0.25 | 0.36 | 0.75 | 4.20 |
| 3 | Circular | 0.836 | 1.0 | 1.36 | 3.45 |
| 4 | Circular | 0.95 | 1.0 | 0.866 | 1.65 |
| 5 | Circular | 2.565 | 3.5 | 4.20 | 6.35 |
| 6 | Rectangular | 1.056 (2.8 × 0.313) | 1.117 (2.8 × 0.35) | 0.325 | 1.85* |
| 7 | Co-axial (C–D outer annulus) | 1.197 | 1.391 (2.075, 1.54) | 1.00 | 1.46* |
| 8 | Circular | 0.25 | 0.302 | 0.512 | 2.91 |
| 9 | Circular | 0.25 | 0.261 | 0.236 | 1.34 |

*See definition in § 4.2.

TABLE 1. Dimensions of nozzles of figure 1.

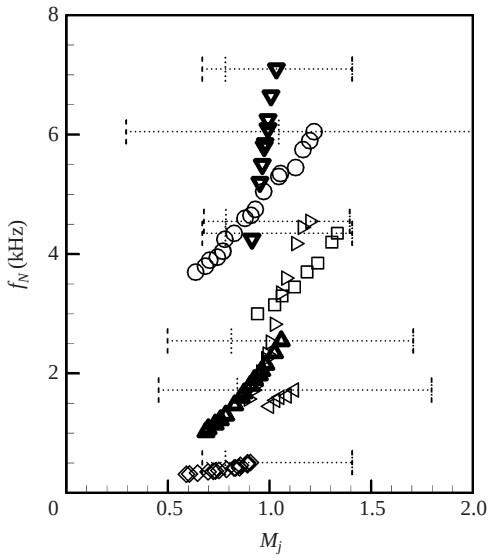


FIGURE 1. Tone frequency variation with $M_j$ for several convergent–divergent nozzles listed in table 1: ○, nozzle 1; □, 2; ◁, 3; ▷, 4; ◇, 5; ▽, 6; △, 7.

in play. The resultant contribution to jet noise may not be negligible; the residual peak in the dashed curve of figure 2 contributed more than 0.5 dB to the overall sound pressure level. Indeed, the phenomenon may be a source of 'internal noise' in nozzle systems. The importance of identifying such a source may be appreciated with regards to jet noise reduction efforts. In the development of a nozzle for modern aircraft, often one has to go to great lengths, with liners on ejector interiors, for example, to absorb internal noise.

Apart from the relevance discussed with the help of figures 1 and 2, the phenomenon may also be pertinent to unsteady transonic flow in various components of a propulsion system. It involves shock/boundary layer interaction followed by an adverse pressure gradient that are also ingredients for '... dynamic distortion in inlets, pressure oscillations in ramjets, buffeting in external flows, and possibly certain types of compressor stalls' (Bogar *et al.* 1983). It is possible that the unsteadiness reported for diffusers (in the cited reference), nozzles (Meier 1974; Hunter 1998), as well as wing sections (Nakamura 1968; Mabey 1981), are of similar origin. Certain rocket

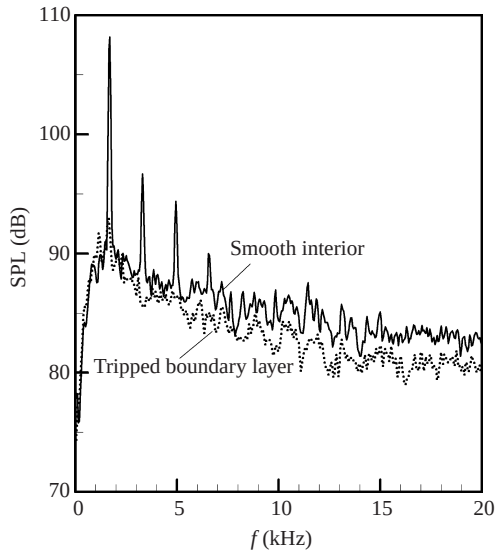


FIGURE 2. Sound pressure level spectra for nozzle 7T1 (nozzle 7 of table 1; co-annular case). Outer jet Mach number, $M_{jo} = 0.86$, inner jet Mach number, $M_{ji} = 1.02$. Boundary layer trip applied to interior of outer nozzle.

engine instabilities (see e.g. Culick 1993) might be coupled to similar unsteady flows in the exhaust nozzle. As will become clear, the flow unsteadiness is internal to the nozzle and, thus, the aerodynamic loads are large. Therefore, this may pose a threat in terms of structural fatigue of nozzles more serious than that posed by conventional screech tones; see Raman (1998) for a discussion of the latter. A continued study of the phenomenon was therefore considered well justified.

In the following, results from single round convergent–divergent nozzles are first considered. The main aim is to advance the understanding of the phenomenon while seeking engineering correlations for prediction of its frequency and methods for its suppression. The experimental procedures are given in § 2. In § 3, salient features of the phenomenon are first discussed. Frequency scaling is then addressed with data from a set of round nozzles having dimensions varied systematically. The time-averaged internal flow is examined via a temperature-sensitive-paint technique and Pitot-static probe measurements. Unsteady flow data, obtained by a miniature pressure probe, are discussed in an effort to shed light on the flow mechanism. In § 4, results from a few past investigations (most involving non-circular geometry) are first discussed; wherever possible, the frequencies of unsteadiness are compared with the correlation equations obtained in this study. Results from a companion numerical simulation are then compared. Finally, in § 5, possible mechanisms are discussed before providing a summary of the investigation. Preliminary results of this investigation have been presented as a conference paper (Zaman, Dahl & Bencic 2001).

## 2. Experimental procedure

The data were obtained in three different jet facilities. In each, compressed air passed through a cylindrical plenum chamber fitted with flow conditioning units and then discharged through the nozzle into the quiescent ambient. The plenum chamber diameters in the three facilities were 30, 10 and 5 in. (Zaman 1999). All experiments

| Nozzle | $D_t$ (in.) | $D_e$ (in.) | $L$ (in.) | $\theta$ (deg.) |
|---|---|---|---|---|
| 1 | 0.307 | 0.400 | 3.00 | 0.89 |
| 2 | 0.304 | 0.400 | 1.50 | 1.83 |
| 3 | 0.300 | 0.400 | 0.75 | 3.81 |
| 4 | 0.304 | 0.400 | 0.48 | 5.71 |
| 5 | 0.300 | 0.400 | 0.375 | 7.59 |
| 6 | 0.300 | 0.320 | 0.75 | 0.76 |
| 7 | 0.300 | 0.500 | 0.75 | 7.59 |

TABLE 2. Dimensions of the nozzles for frequency-scaling study.

involved 'cold' flows, i.e. the jet was unheated and the total temperature everywhere was approximately the same as the ambient temperature.

In table 1, nozzles 3–7 were made of aluminium and the rest were made of clear plastic. The aluminium nozzles had a 'normally' machined surface finish. The surface 'roughness height deviation' in most cases was about 64 microinches. Some of the plastic nozzles were polished to enable visualization of the internal flow. The roughness height deviation in those cases was about16 microinches. Nozzles 3, 4, 8 and 9 were designed following the method of characteristics. In other cases, less rigorous criteria were followed. The throat-to-exit axial length ($L$) and the half-angle of divergence ($\theta = \tan^{-1}((D_e - D_t)/2L)$) are used to characterize the overall geometry of the divergent section. Here, $D_e$ and $D_t$ are the exit and throat diameters, respectively. The half-angle $\theta$ for the rectangular (6) and co-annular (7) nozzles are defined in § 4.2.

In order to address frequency scaling, a set of plastic nozzles was fabricated. All had identical convergent sections and a nominal throat diameter, $D_t = 0.3$ in. The divergent section was a straight cone starting at 0.050 in. from the throat; the transition was faired smoothly. While keeping $D_t$ a constant, $L$ and $D_e$ were varied. The dimensions of the divergent section of these nozzles are given in table 2. (In the following a given nozzle will be identified by its number followed by the table number; e.g. '3T2' will denote nozzle 3 of table 2.) Some of the nozzles had to be re-surfaced and repolished in order for the resonance to take place prominently. This explains the somewhat larger throat diameter for some cases. In addition to the nozzles listed in table 2, another set of experiments was conducted starting with nozzle 2T2 and then trimming it off in steps to provide lengths of 1.3, 1.1, 0.9, 0.75, 0.6 and 0.495 in. Thus, for this set both $L$ and $D_e$ varied but $\theta$ remained approximately a constant (actually, $\theta$ decreased somewhat for small $L$ due to the fairing near the throat). Various combinations permitted an examination of the parametric dependence of the resonant frequency.

The frequency data were obtained from spectral analysis of the sound pressure measured with a microphone. The bandwidth was chosen such that the accuracy of the measured tone frequency was within 1%. The 'jet Mach number',

$$M_j = \left( ((p_0/p_a)^{(\gamma-1)/\gamma} - 1) \frac{2}{\gamma - 1} \right)^{1/2},$$

is used as the independent variable. Here, $p_0$ and $p_a$ are plenum pressure and ambient pressure, respectively. The uncertainty in the measurement of $M_j$ is also well within 1%. Some other experimental procedures will be discussed along with the results.

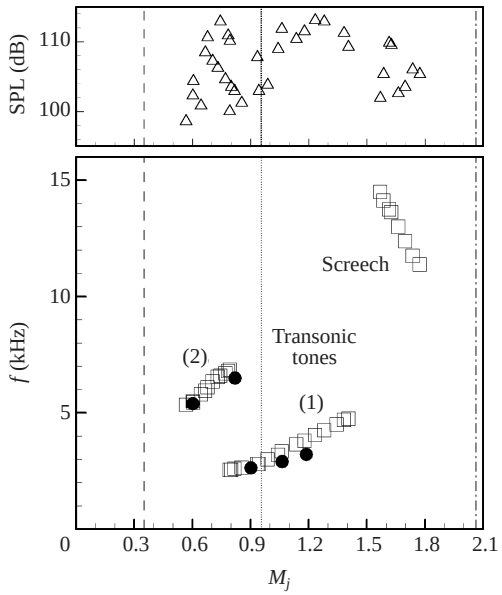


FIGURE 3. Variation of frequency (□) and amplitude (△) of tones with $M_j$ for nozzle 3T2 ($D_t = 0.3$, $D_e = 0.4$, $L = 0.75$). Solid circles from numerical simulation (§4.3).

## 3. Results

### 3.1. *Distinction from screech tones*

Salient features of the resonance and its difference from conventional screech tones are summarized in figures 3–6. Variations of frequency and amplitude of the tone for nozzle 3T2 are shown in figure 3. The band of frequency data on the right represents screech tone. This is recognized as such from the characteristic variation (frequency decreasing with increasing $M_j$) and also from a comparison of the Strouhal number with data from the literature. The 'transonic resonance' takes place in two stages, as represented by the two bands of frequency data on the left. These are marked (1) and (2) in the figure. A difference in the trend is immediately apparent. Unlike screech, the frequency in both stages increases with increasing $M_j$. Another important and pertinent distinction is that the 'transonic tones' occur only with C–D nozzles and not with a convergent nozzle. In contrast, screech tones, in fact, have been studied mostly with choked flows from convergent nozzles. The solid symbols represent frequency data obtained from a computational study that will be discussed in §4.3. The amplitude data shown at the top of figure 3 demonstrate that the transonic tones are loud, often louder than the screech tones.

In figure 3, the vertical lines demarcate flow regimes determined from one-dimensional nozzle flow analysis, based simply on the throat-to-exit area ratio. From the left, the first (dashed line) represents the condition when the flow is just choked, the second (dotted line) when a 'normal shock' is expected at the nozzle exit, and the third (chain-dashed line) when the flow is perfectly expanded. Thus, to the left of the dashed line the flow is subsonic, between the dashed and dotted lines a shock is expected in the divergent section, between the dotted and the chain-dashed lines the flow is overexpanded, and to the right of the chain-dashed line the flow is underexpanded. (These regimes were also marked for each dataset in figure 1.) It appeared from the boundaries in figure 3 that the resonance could take place when a shock existed

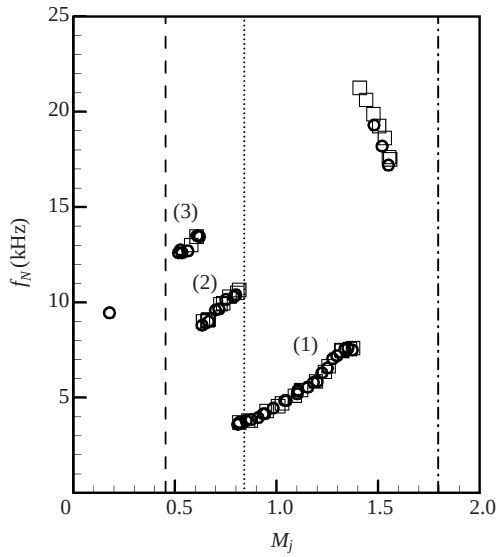


FIGURE 4. Tone frequency variation for nozzle 8T1 ($D_t = 0.25$, $D_e = 0.302$, $L = 0.512$): □, data from a small jet facility; ○, data from a large jet facility.

within the divergent section or when the flow was in the early stage of overexpansion. However, it will be shown later that one-dimensional analysis grossly underpredicts the location of the 'dotted' boundary, and the resonance always involves a shock within the divergent section.

Frequency data for nozzle 8T1 are shown in figure 4. The band of data on the right again represents screech. Here, three stages are observed for the transonic tones. There are overlaps between stages where peaks at both frequencies occur in the time-averaged spectrum; the frequencies are not exact harmonics of each other. The square and circular symbols represent data taken in two jet facilities with the same nozzle. It is clear that the transonic tones are independent of the facility and characteristic of the nozzle. Occasionally, tones would occur when the flow was entirely subsonic; one such data point is shown to the left of the dashed vertical line. These appeared to be related to facility resonance or other unknown sources and are ignored for the rest of the paper. Most nozzles exhibited two stages of the transonic resonance. Stage (1) was typically persistent and involved the loudest tones. Data for only this stage were shown in figure 1. (It is worth mentioning here that often a minute change in $M_j$ would not change $f_N$; thus, on a finely resolved abscissa, the frequency varied in a step-like rather than continuous fashion within a given stage.)

Figure 5 shows sound pressure level spectra for nozzle 9T1. Data for three values of $M_j$ are shown, there being a pair of traces at each $M_j$. The dotted lines represent the case with two 'tabs' installed at the nozzle exit (Samimy, Zaman & Reeder 1993). While screech is eliminated by the tabs (at $M_j = 1.58$), the transonic tones at the two lower $M_j$ are affected just slightly. In fact, the small effect (somewhat lower frequency and amplitude) could be due to blockage by the tabs. It was noted that a relatively large tab (e.g. the end of a flat-headed screwdriver inserted sufficiently into the flow) would eliminate the tone completely. But this apparently occurred due to a shift of the choke location to the exit, when the nozzle acted like a convergent one. Results of figure 5 suggest that the origin of the tone under consideration is internal to the nozzle, and this is confirmed by the boundary layer trip effect.

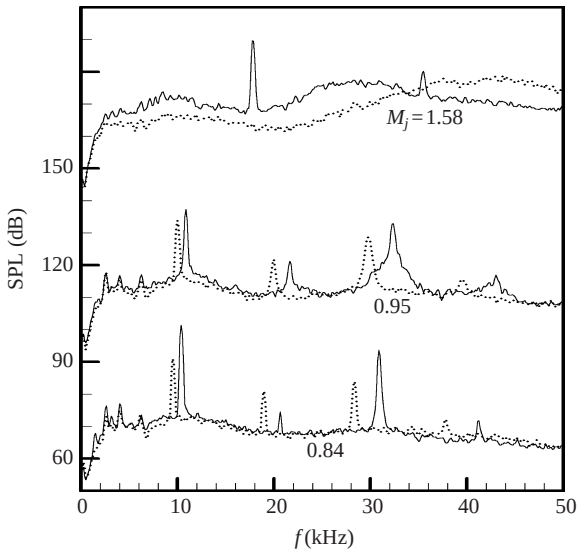


FIGURE 5. Sound pressure level spectra for nozzle 9T1 ($D_t = 0.25$, $D_e = 0.261$, $L = 0.236$). Three pairs of spectra, staggered by 40 dB, are for the indicated values of $M_j$ (ordinate pertains to the pair at the bottom). Solid curves, normal operation; dotted curves, with two tabs at the exit.

### 3.1.1. *Effect of boundary layer trip*

Sound pressure level spectra, with and without boundary layer trips, are shown in figure 6 for nozzle 4T1. Data for three values of $M_j$ are presented in the same manner as in figure 5. The trip was composed of four $\frac{1}{2}$ in. wide pieces of adhesive tape (approximately 0.003 in. thick) placed close to but sufficiently upstream of the throat so that there was no change in the minimum area. These were spaced equally around the periphery. It can be seen that, at the highest $M_j$, there is no effect on screech. This is expected because screech occurs due to a feedback loop external to the nozzle. However, the trip essentially eliminates the transonic tones in this case, at the lower values of $M_j$. A similar result was shown for nozzle 3T1 (Zaman & Dahl 1999) as well as for nozzle 7T1 (figure 2).

The effect of boundary layer trip location was explored further with nozzle 3T1. The observations were only qualitative but narrated here because of their practical significance. (A robust engineering solution for the suppression of the resonance should require elaborate testing that was considered outside the scope of this study.) Four epoxy beads, each approximately 0.08 in. across and 0.005 in. high, were placed at a given axial location spaced equally on the internal wall. The tone amplitudes were measured at two operating conditions: $M_j = 1.0$ ($f_N = 1.55$ kHz) and $M_j = 0.89$ ($f_N = 3.6$ kHz). When the beads were located 0.3 in. upstream of the throat the amplitudes reduced by about 80%; however, small but clear peaks remained in the spectrum. Almost a complete suppression was achieved when the beads were located about 0.3 in. downstream of the throat. At the latter location, however, the effect was inconsistent at other values of $M_j$ (tone reappeared). On the other hand, when the beads were moved farther downstream the effectiveness diminished rapidly. It appeared that the trip needed to be placed close but prior to the location of the shock in order to achieve the best suppression. Furthermore, during these as well as the temperature-sensitive-paint (§ 3.3) experiments, it appeared that the resonance was more susceptible to azimuthal non-uniformity of the trip. That is, the same roughness

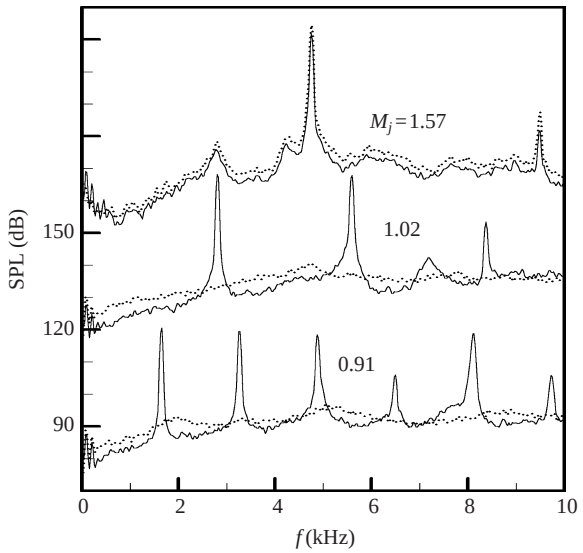


FIGURE 6. Sound pressure level spectra as in figure 5 for nozzle 4T1 ($D_t = 0.95$, $D_e = 1.0$, $L = 0.866$): solid curves, smooth interior of nozzle; dotted curves, tripped boundary layer.

placed at a few azimuthal locations rather than uniformly over the periphery appeared to be more effective in the suppression. It was also noted that the trip affected the amplitude but seldom the frequency of the tone. The amplitude was indeed sensitive to the surface texture near the throat. For example, when the trips were removed, smudges inadvertently left behind would affect the tone and the amplitude would not reproduce exactly.

### 3.2. *Frequency scaling*

Parametric dependence of the frequency of the transonic tone is now addressed. At first, data for only stage 1 is considered. Figure 7 shows data for the 'trimmed' cases. The length of the divergent section $L$ is varied while $\theta$ remains approximately constant. The frequency data have been non-dimensionalized as $f_N L/a_0$, where $a_0$ is the speed of sound in the ambient (a constant). First, it is noted that in each case, there is approximately a linear variation of frequency, with the exception that for small values of $L$ there is a clear departure from linearity at either end of the curve. Ignoring this departure, there is a good overall collapse of all the data. Thus, it is apparent that the resonant frequency, to a first approximation, simply scales inversely as the length of the divergent section. This observation, however, conflicts with the trend of another set of data shown in figure 8. Non-dimensionalized frequencies are shown, again, for varying $L$ while $D_e$ is held constant (nozzles 1–5 of table 2). It can be seen that the curves are close together for small values of $L$ but there is very large departure with increasing $L$. This posed a stumbling block in the understanding of the frequency scaling for a long time. It was not clear if the departure for large $L$ was due to a 'staging' behaviour or some other factor.

After inspection of many sets of data, it became apparent that the frequency curves had a systematic dependence on the parameter $\theta$. In figure 8, $\theta$ decreases with increasing $L$. The slope of the frequency curve steepens with decreasing $\theta$. In figure 7, for small values of $L$, $\theta$ also decreases somewhat due to the fairing near the throat. A somewhat steeper slope of the frequency curves can also be noticed

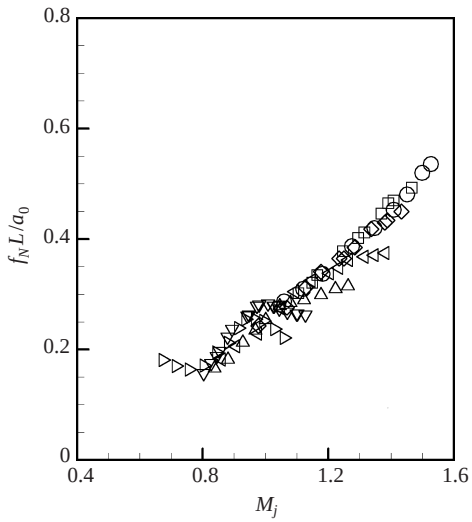


FIGURE 7. Frequency variation (stage 1) for nozzle 2T2 ($D_t = 0.304$) trimmed to different lengths: ○, $L = 1.5$; □, 1.3; ◇, 1.1; ◁, 0.9; △, 0.75; ▽, 0.6; ▷, 0.495.

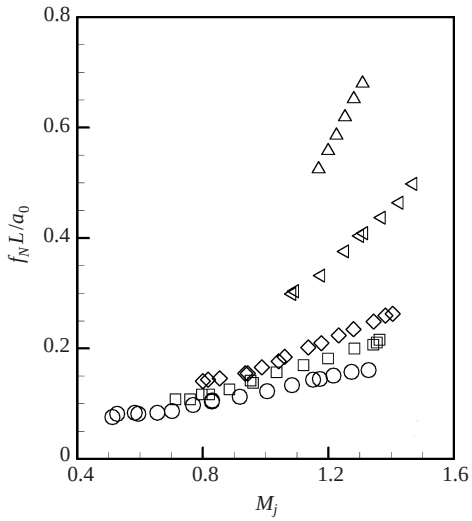


FIGURE 8. Frequency variation (stage 1) for nozzles of constant throat and exit diameters ($D_t \approx 0.3$ and $D_e = 0.4$) but different throat-to-exit length $L$ (table 2). △, 3.0 (nozzle 1); ◁, 1.5 (2); ◇, 0.75 (3); □, 0.48 (4), ○, 0.375 (5).

for the smallest values of $L$. Finally, data for varying $D_e$, with $L$ held constant, are shown in figure 9. Increasingly steeper slope can be observed for decreasing $D_e$ that is accompanied by decreasing values of $\theta$. One might try other parameters in the non-dimensionalization, e.g. diameter as a length scale, but it is clear that no other combination would readily account for the changes in the slopes. The change of slope apparently relates to differences in the rate of divergence suffered by the flow. An average measure of the latter is given by the parameter $\theta$. The $\theta$-dependence of the frequency curves is discussed shortly.

First, the staging behaviour is examined. Four examples of the frequency variation over the full range of $M_j$ are shown in figure 10($a$–$d$). In each part, the dimensional

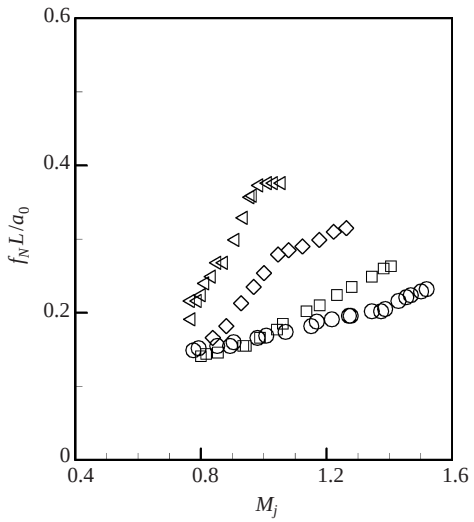


FIGURE 9. Frequency variation (stage 1) for nozzles of constant $D_t$ and $L$ but different $D_e$ (table 2). ○, 0.5 (nozzle 7); □, 0.4 (3); ◇, 0.35 (2, trimmed); ◁, 0.32 (6).

data are shown on the top. There are three stages in figure 10(*a*), two each in figures 10(*b*) and 10(*d*), and only one in figure 10(*c*). Between cases (*b*) and (*d*) there is an order of magnitude difference in the frequencies, commensurate with an order of magnitude difference in nozzle dimensions. After inspection of all data it becomes apparent that stage 1 is indeed the fundamental in the resonance, stages 2 and 3 being the next odd harmonics. That is, with decreasing $M_j$, at the left end of stage 1, there is an increase in the frequency by approximately a factor of 3 to begin stage 2. Similarly, at the left end of stage 2, the onset of stage 3 involves a jump by a factor of about 5/3. This becomes clear from the non-dimensional data shown at the bottom of each figure (ordinate on right), with appropriate 'stage correction'. That is, frequencies in stages 2 and 3 have been divided by factors of 3 and 5, respectively. In this way, the best collapse of all stages to a single curve was achieved. There is a perceptible discontinuity between stages 1 and 2; however, stages 2 and 3 in (*a*) blended quite well.

That the higher stages are odd harmonics of the fundamental follows acoustic resonance characteristics of the divergent section (without flow). For a conical duct 'driven' from the smaller end and open at the other, a fundamental acoustic resonance would correspond to a standing one-quarter wave, with higher 'stages' occurring at only the odd harmonics. The resonant frequencies can be calculated as (see e.g. Morse 1948)

$$f_m = \frac{a_0}{4l_p}\sqrt{m^2 + \frac{8l_p}{\pi^2 x_0}}, \quad m = 1, 3, 5\ldots, \tag{1}$$

where

$$l_p = L + \frac{4D_e}{3\pi}, \quad x_0 = \frac{D_t}{2\tan\theta}.$$

The fundamental frequencies for the four cases of figure 10, given by equation (1), are: (*a*) 7.80, (*b*) 0.70, (*c*) 3.91and (*d*) 2.28 kHz. While the calculated value lies within the ranges of frequencies in (*b*) and (*c*), it is outside the ranges in (*a*) and (*d*). Note that the acoustic resonance frequencies are constants. For the subject phenomenon,

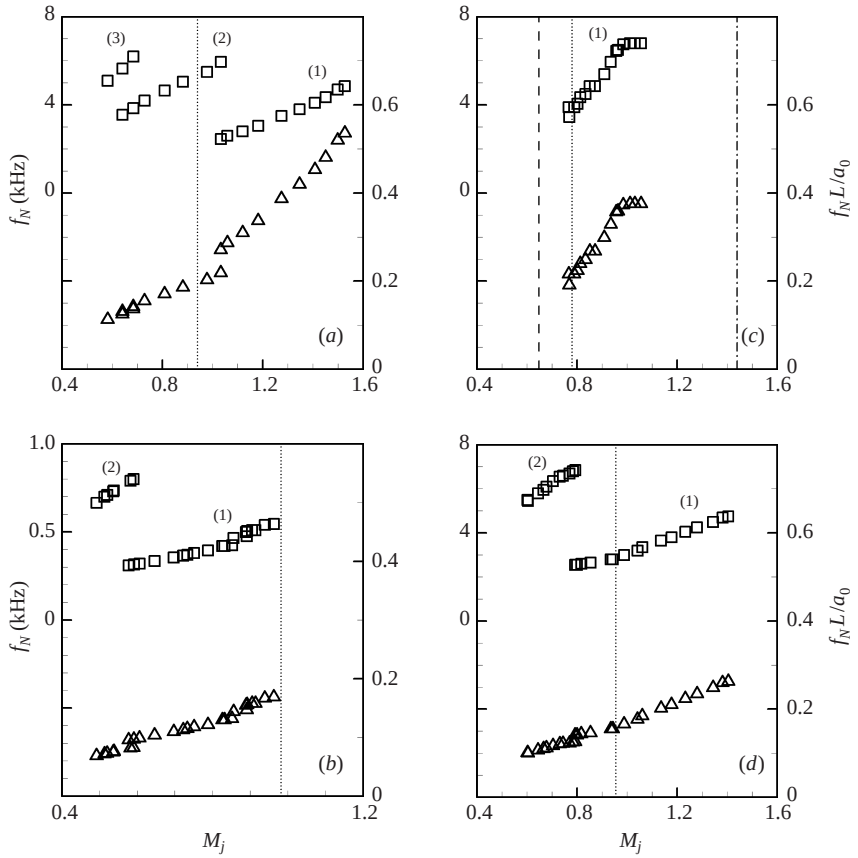


FIGURE 10. Frequency variation (full range) for four different nozzles. Dimensional data (□) are at the top, corresponding non-dimensional data (△) with 'stage correction' are at the bottom; numbers in parentheses are stages. (*a*) Nozzle 2T2, (*b*) 5T1, (*c*) 6T2, (*d*) 1T1.

frequency varies within a stage. Thus, the transonic tones are not merely 'acoustic resonance' excited by the flow. The flow field, which is very complex, comes into play. Nevertheless, the occurrence of only the odd harmonics suggests that the underlying mechanism must be similar to that of acoustic resonance. This is addressed further later in the text.

In order to examine the $\theta$-dependence, $f_N L/a_0$ versus $M_j$ curves are constructed for all (single round) nozzle cases in the same way as in figure 10. A total of seventeen cases, from tables 1 and 2 and the trimmed cases of figure 7, are included in this exercise in an effort to find a correlation. The frequency variation in each stage is assumed to be linear. The slopes are estimated by drawing straight lines through the data in each stage. (The data on the ends of a stage departing from linearity are ignored in this process. A few cases with very small $\theta$ have not been included since a linear part in the curve is not readily discernible.) Simultaneously, the intercepts at $M_j = 1$ are also obtained. When all the data are plotted a consistent dependence on $\theta$ emerges. The dependence of the slopes can be seen clearly in figure 11. Data for stage 1 are shown by the triangular symbols while those for stages 2 and 3 are shown by the circular symbols. In a given stage, the slopes vary inversely as $\theta$. The intercepts also exhibit an inverse functional dependence on $\theta$, as shown in figure 12.

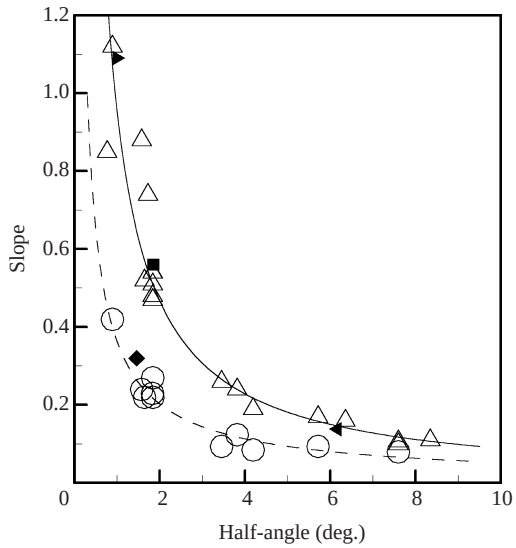


FIGURE 11. Slope of $f_N L/a_0$ versus $M_j$ for various nozzles, as a function of the half-angle of divergence ($\theta$); △, stage 1; ○, stages 2 and 3; ■, nozzle 6T1; ◆, nozzle 7T1; ►, Bogar *et al.* (1983); ◄, Hunter (1998).

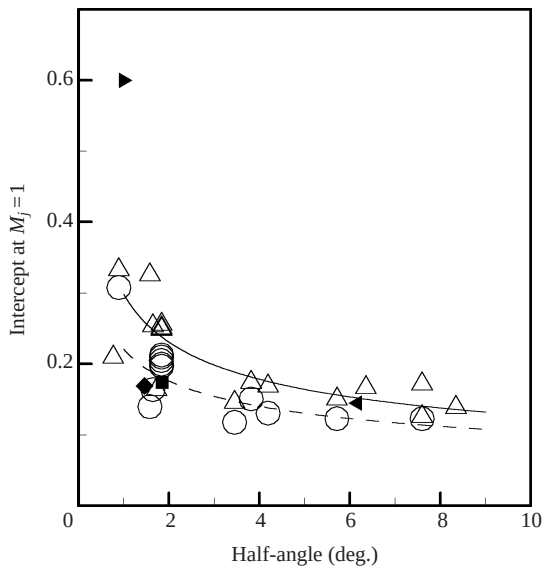


FIGURE 12. Intercepts at $M_j = 1$ corresponding to the cases of figure 11.

The curves in figures 11 and 12 are least-squares-fits through the data for the round nozzle cases (open symbols).

From the fitted curves the following equation is obtained, with $\theta$ expressed in degrees:

$$\frac{f_N L}{m a_0} = C_1(\theta) + C_2(\theta)(M_j - 1), \quad m = 1, 3, 5 \ldots, \tag{2}$$

where $C_1(\theta) = 0.298\theta^{-0.370}$, $C_2(\theta) = 0.952\theta^{-1.029}$ for stage (1), and $C_1(\theta) = 0.221\theta^{-0.325}$, $C_2(\theta) = 0.363\theta^{-0.8375}$ for stage (2).

The frequency for stage 3 ($m = 5$) is also given by the equation for stage 2. The value of $M_j$ where the jump from stage 1 to 2 takes place also appears to depend on $\theta$ and is given by curve-fit, $(M_j)_{1-2} = 1.036\theta^{-0.157}$. These correlation equations would allow one to estimate the resonant frequency at any $M_j$ simply from the dimensions $L$ and $\theta$. Recall that the amplitude of the resonance is not well defined and is sensitive to e.g. the surface finish of the nozzle's interior. Thus, no attempt is made to correlate the amplitudes.

The solid data points in figures 11 and 12, identified in the captions, are for rectangular and co-annular nozzles. It is obvious that equation (2) also predicts these data quite well. A discussion of this is deferred to § 4.2.

### 3.3. *Steady-state internal flow characteristics*

Time-averaged internal flow structure is discussed in this section based on wall-temperature and centreline pressure distributions. These steady-state results should provide a clearer perspective of the internal flow field with and without the resonance, for the more serious reader with a close interest in related research areas. A reader with only general interest may consider a cursory perusal, review figures 13–17, and move on to § 3.4.

#### 3.3.1. *Wall temperature*

The temperature-sensitive-paint technique was used for these measurements. The paint was sprayed on a 'sector' of the interior of the divergent section. The painted strip extended from about the throat to the exit, and the layer was initially about 0.001 in. thick. The non-uniformity in the layer was enough to trip the boundary layer for some of the nozzles, resulting in a 'dulling' of the tones. The painted surface had to be polished in order to get the sharp tones back. The picture of the painted strip was taken from outside with a CCD camera. Under filtered blue light (460 nm) the emission intensity from the paint responded to the static temperature. Two images were taken – one without flow and another with flow. The data were post-processed by normalizing the level in each pixel for flow with the corresponding no-flow level. Temperature differences, as small as a fraction of a degree, could be discriminated by the technique (Liu *et al.* 1997).

Figure 13 shows images of the temperature distribution for nozzle 3T2 at different $M_j$. The pictures on the left are for a tripped boundary layer (resonance suppressed). The pictures on the right are the corresponding cases with a smooth interior (resonance on). Bands of colour indicating regions of temperature gradients are observed. For the tripped case, strong gradients are observed approximately in the middle of the divergent section. The sharp edge on the right of the dark blue region apparently indicates the location of the shock. In general, lower temperatures are expected in regions of high-speed attached flow while higher temperatures are expected past a shock and with boundary layer separation. With resonance, the right column, the distributions are seen to change significantly. At $M_j = 0.86$, 1.06 and 1.19, a warm band (in red and yellow) is observed. This apparently corresponds to a separation bubble. Note that these three $M_j$ cases represent resonance in stage 1 while at $M_j = 0.67$ resonance in stage 2 takes place (figure 3).

Temperature profiles, along an axial line in the middle of the visualized sector, are shown in figures 14 and 15 for the tripped and untripped cases, respectively. Some of the profiles are annotated for easy reference. Note that $x^*$ represents the throat location, so that 1.0 on the abscissa represents the nozzle exit. Let us first examine the trends in figure 14. The temperature is seen to decrease with increasing distance

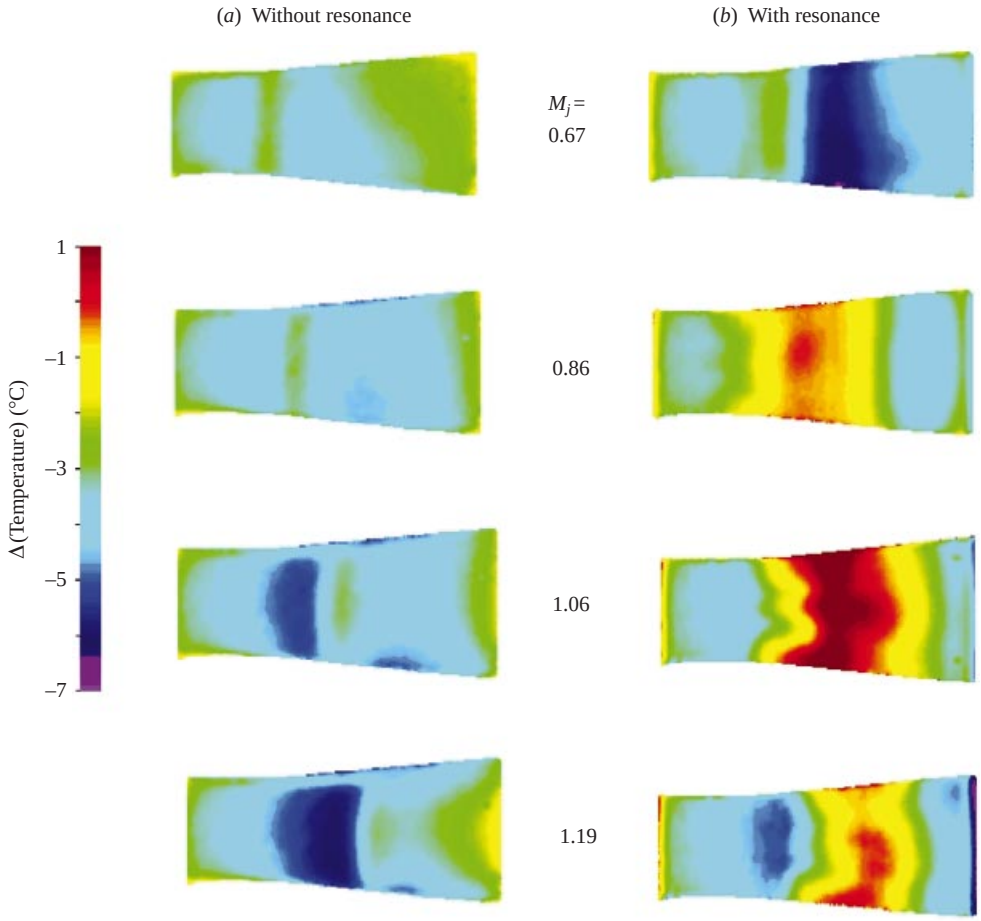


FIGURE 13. Interior wall temperature distribution for nozzle 3T2 ($D_t = 0.3$, $D_e = 0.4$, $L = 0.75$), at the indicated values of $M_j$. (*a*) for tripped boundary layer, (*b*) for smooth interior.

from the throat until at a certain downstream location a relatively abrupt increase takes place, at the location where the 'foot' of the shock intersects the wall. Upstream of this, the flow is supersonic and the Mach number gradually increases from unity at the throat to some higher value as the shock is approached. The increasing Mach number is accompanied by decreasing static temperature.

The static temperature, however, can be calculated to be much lower than the recorded temperatures (Δ (temperature) represents static temperature relative to ambient temperature). For example, for a Mach number of 1.2, likely in many of the cases of figure 14, Δ (temperature) would be about −35 °C. This contrasts with the measured values, which are no lower than −7 °C. This difference is due to the fact that the data represent 'wall temperature' that ideally should be equal to the total temperature (see e.g. Schlichting 1979). In practice, however, there are radiation and conduction losses and the wall temperature is always less than the total temperature. For a thermal boundary layer (Crocco–Buseman equation, see Schlichting 1979), this is accounted for by a 'recovery factor'. With the assumption of a constant recovery factor, it follows that the relative variation in wall temperature is the same as that in

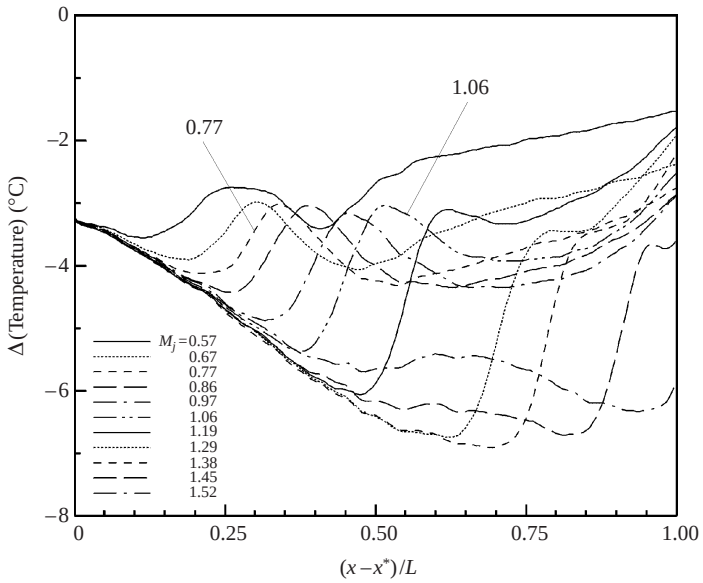


FIGURE 14. Axial variation of wall temperature corresponding to the tripped cases of figure 13 (resonance suppressed) for the indicated values of $M_j$.

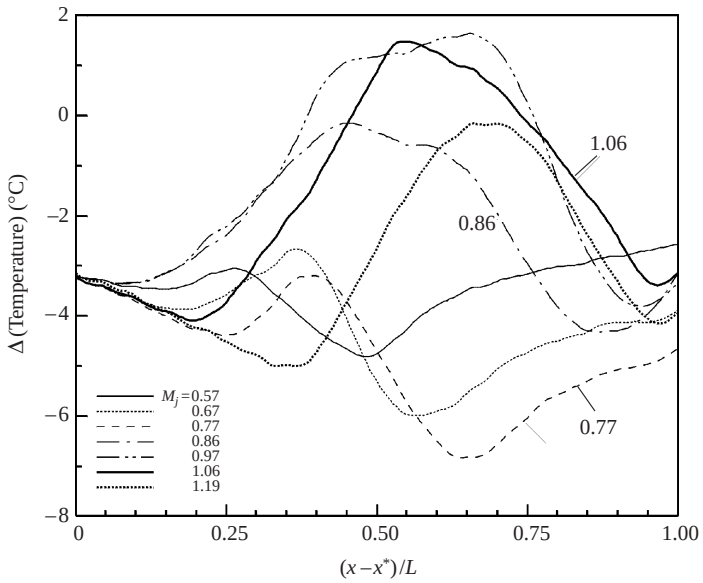


FIGURE 15. Axial variation of wall temperature for the cases with smooth interior of figure 13 (with resonance).

core static temperature, although the magnitude of the former is only a fraction of the latter.

Since the core static temperature is proportional to the static pressure, it follows that the measured temperature profiles are similar to the static pressure profiles. In fact, the overall trends in the temperature profiles of figure 14 bear striking similarity to static pressure profiles reported by e.g. Anderson (1982) and Hunter (1998). The

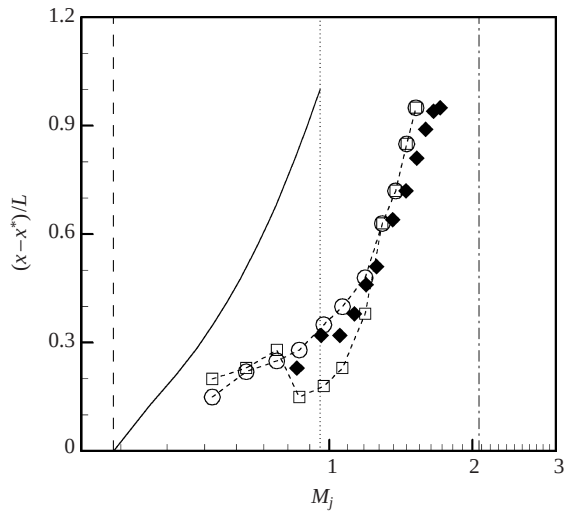


FIGURE 16. Shock location versus $M_j$. Circular and square data points are inferred from figures 14 and 15; ○, tripped case; □, smooth interior. ◆, From wall static pressure data for a rectangular C–D nozzle (Hunter 1998). The solid line on the left represents the prediction from one-dimensional analysis.

static pressure also drops with increasing distance from the throat and then rises abruptly past the shock. In the cited references the shock location was defined by the location of minimum static pressure before the abrupt rise. A similar criterion is applied here to determine the shock location from the temperature minima.

Shock locations for the tripped case (figure 14), obtained by the stated criterion, are plotted in figure 16 (circular data points). The abscissa is logarithmic, and unity on the ordinate represents the nozzle exit. It can be seen that the shock moves downstream with increasing $M_j$, and reaches the exit at $M_j \approx 1.55$. Also shown in figure 16 is the theoretical prediction for the shock location based on one-dimensional analysis (solid curve between the dashed and dotted vertical lines). It becomes clear that the shock actually resides within the nozzle at pressure ratios (or $M_j$) much higher than that predicted by one-dimensional analysis. The 'dotted' boundary in reality is at $M_j \approx 1.55$ instead of 0.955. A similar inference is made from published static pressure data, for example from Hunter's (1998) rectangular nozzle data shown by the solid diamond symbols in figure 16, as well as from the classical 'Stodola experiment' described by Anderson (1982) for a circular nozzle. (The dimensions of Hunter's nozzle were such that the predicted flow regime boundaries were practically identical to those in figure 16 for nozzle 3T2.)

Referring back to figure 15, it can be seen that, with the onset of resonance, the temperature distributions are no longer orderly. The shock location (temperature minimum) at a given $M_j$ has moved upstream. However, a second temperature minimum occurs downstream. For example, at $M_j = 1.06$, the shock has moved from $0.35L$ (figure 14) to $0.2L$ (figure 15); this shift can also be seen in figure 16 from the square data points. Besides the temperature minimum at $(x - x^*) = 0.2L$, there is another minimum close to the exit. With the assumption that the latter is the location of boundary layer reattachment, one infers that a separation bubble, in a time-averaged sense, exists under the resonant condition. The bubble is long at the three higher $M_j$ cases that involve resonance in stage 1. In comparison, the second temperature-minimum occurs further upstream at the three lower $M_j$ cases that

involve resonance in stage 2. Thus, a shorter separation bubble is involved in stage 2 while in stage 1 the bubble length is comparable to $L'$, the distance of the nozzle exit from the shock. (The wall temperature for a few cases in figure 15 is somewhat in excess of the ambient temperature. This is thought to be due to dissipation within the separation bubble.)

The data presented in this section clarify an aspect of the resonance. Initially, from the data in figures 1, 3 and 4 it was thought that the resonance might be possible even without a shock inside the divergent section (the resonance extended well into the 'overexpanded' regime predicted by one-dimensional analysis). The results discussed here make it amply clear that for the subject flow a shock still resides inside the nozzle. In fact, it is apparent from accumulated evidence that the presence of a shock approximately within the upstream half of the diverging section is a necessary condition for the occurrence of the resonance.

3.3.2. *Centreline pressure distributions*

Static and total pressure measurements were carried out in nozzle 5T1 with a Pitot-static probe. The outer diameter of the probe was $d = 0.094$ in. The large size of the nozzle enabled the measurements to be taken without significant probe interference. The data were obtained on the centreline of the nozzle starting immediately downstream of the throat. Two flow conditions were chosen: (a) $M_j = 0.55$ yielding a resonant frequency of 755 Hz (stage 2), and (b) $M_j = 0.75$ yielding a resonant frequency of 385 Hz (stage 1); the frequency data for this nozzle have been shown in figure 10(*b*).

The static pressure taps were located about $11d$ from the tip of the probe. In supersonic flow with a streamwise pressure gradient there are ambiguities in static pressure measurements. In particular, the location of the measured pressure relative to the probe tip is subject to question and depends on the precise geometry of the probe. It was assumed that the free-stream static pressure ($p_1$; in standard normal shock notation, see e.g. Ames Staff Report 1953) was measured at the location of the taps. The Pitot probe, on the other hand, yielded the total pressure downstream of the probe-induced shock ($p_{t2}$). The Rayleigh–Pitot formula was applied to calculate shock Mach number ($M_1$) that in turn yielded the free-stream total pressure ($p_{t1}$). These pressure distributions, denoted by $p_t(= p_{t1})$ and $p_s(= p_1)$, are shown in figure 17 for the two operating conditions. These data are included in spite of some measurement ambiguities because they describe the basic state of the flow for the two operating conditions for which unsteady flow data are presented in the next subsection. Note that most of the data are for the subsonic regime downstream of the shock where the measurements are free from the stated ambiguities.

The trend in the static pressure data of figure 17 is similar to that observed from wall-pressure data, as discussed earlier in this subsection. The shock location, denoted by the minimum before the sharp rise in the pressure, is at $x/L = -0.9$ and $-0.8$ at $M_j = 0.55$ and 0.75, respectively ($x$ is referenced to the nozzle exit). The total pressure data exhibit a drop-off near the location where static pressure rises. A close inspection reveals some discrepancy. Consider the curves for $M_j = 0.75$ (circular symbols). It is reasonable to assume that the total pressure drop (over $x/L = -0.9$ to $-0.75$) takes place over the shock. The drop across the shock ($p_{t2}/p_{t1} = 0.97$) would indicate a shock Mach number ($M_1$) of about 1.35. However, the ratio of static pressure rise over the same distance ($p_2/p_1$) is about 1.5. The latter would indicate a shock Mach number of 1.2. The source of this discrepancy is not completely clear. However, it is thought to be due to the fact that the shock is not steady. As we will see, there

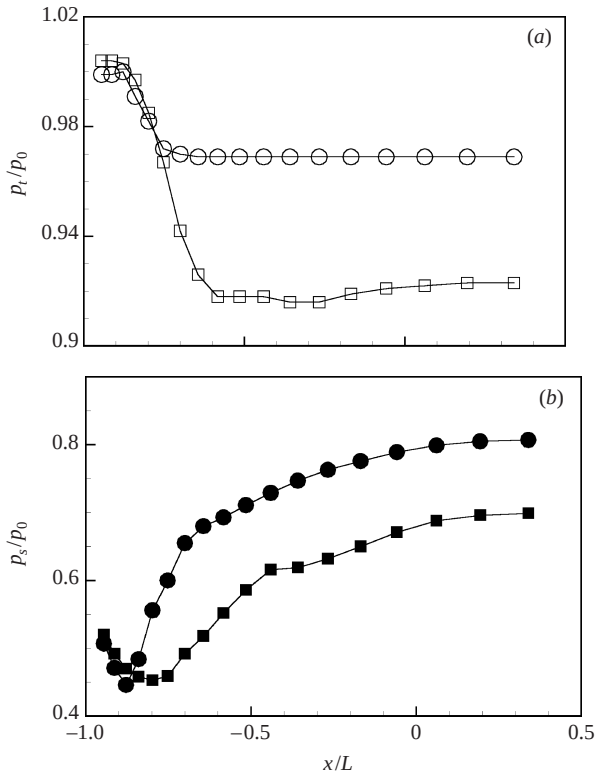


FIGURE 17. Centreline variations of (*a*) total pressure and (*b*) static pressure for nozzle 5T1 ($D_t = 2.565$, $D_e = 3.5$, $L = 4.2$): □, ■, $M_j = 0.55$ ($f_N = 755$ Hz); ○, ●, $M_j = 0.75$ ($f_N = 385$ Hz).

are large changes in the shape and strength of the shock over the oscillation cycle. Thus, normal shock relationships may not apply. In fact, when the boundary layer was tripped to suppress the resonance, yielding a steady shock, the drop in total pressure was found to be much less. The shock Mach number calculated from the total pressure then agreed closely with that obtained from the static pressure rise. A similar observation was also made for the other $M_j$ case.

### 3.4. *Unsteady flow characteristics*

The unsteady flow characteristics were explored with a miniature pressure transducer for nozzle 5T1 for the two flow conditions stated in the previous section: $M_j = 0.55$ (755 Hz; stage 2), and $M_j = 0.75$ (385 Hz; stage 1). The transducer was mounted on a 9 in. long support that telescoped from a root diameter of 0.25 in. to the sensor diameter of 0.063 in. It was inserted straight into the flow (as with a Pitot probe) from a streamlined support mounted on the probe traversing mechanism. The probe essentially responded to unsteady total pressure. A $\frac{1}{4}$ in. (B&K) microphone, placed just outside the flow and near the lip of the nozzle, provided a reference signal for the measurements.

Radial profiles of the phase (i.e. 'mode shape' at the resonant frequency), are shown in figure 18. The data are for a streamwise location just downstream of the nozzle exit. The phase is measured through spectrum analysis of the transducer signal, relative to the fixed microphone signal. Ignoring some details, it is clear that the resonance at either stage involves axisymmetric fluctuation. As reported by Zaman & Dahl

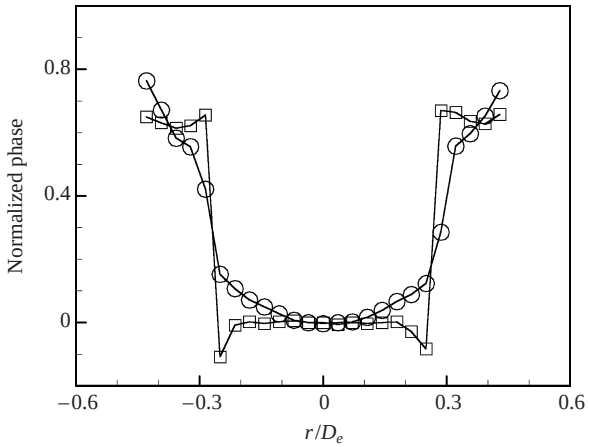


FIGURE 18. Radial profiles of the phase at $x/D_e = 0.25$ for nozzle 5T1: □, $M_j = 0.55$ ($f_N = 755$ Hz); ○, $M_j = 0.75$ ($f_N = 385$ Hz).

(1999), cursory measurements with several other nozzles and operating conditions also indicated axisymmetric shapes. The rectangular nozzle case included in figure 1 also involved a symmetric shape.

The phase-averaged amplitude of the unsteady total pressure was measured at various axial locations on the nozzle centreline. At each location, the data were recorded for 39 time steps (phases) covering about $1.2T$, $T$ being the period of the resonance. Sample data for the flow inside the nozzle are shown in figures 19($a$) and 19($b$) for $M_j = 0.55$ and 0.75, respectively. The ordinates are approximately in percentage of the plenum pressure. One finds that quite large fluctuations take place – as much as $\pm 20\%$ in stage 1 at $M_j = 0.75$ in ($b$). Thus, the nozzle is subjected to very large unsteady aerodynamic loads under the resonant condition.

The data in figure 19 cover an axial range from $x/L = -0.6$ to about the nozzle exit. Upstream of this range, the amplitudes drop rapidly. There, the small amplitudes are contaminated by probe interference, especially when the probe is near the shock (evident from changes in the reference signal). Thus, the measurements could not be carried out in those regions. In each of figures 19($a$) and 19($b$), the waveforms are complex. They are far from sinusoids and there is large harmonic distortion. While the processes leading to these waveforms and the details of the unsteady shock motion remain unclear, an important aspect of the flow becomes apparent from these data. There is relatively little phase shift within the measurement range, especially for stage 1 in figure 19($b$). The phase shift for stage 2 (figure 19$a$), up to about $x/L = -0.31$, is also small. The lack of phase shift indicates that these are standing waves within the nozzle. If the data in figure 19($b$), for example, represented travelling wave and the $x$-range covered corresponded to $\frac{1}{4}$ wavelength, the curves marked '1' and '0' would be separated by $t/T = 0.25$. This is not the case and for a portion of the period the curves are bunched together. The standing wave characteristics are further discussed in § 4.3.

## 4. Comparison with past experiments and numerical simulation results

### 4.1. *Past experiments*

Past experiments that showed a similar unsteady flow through nozzles at 'transonic conditions' are discussed here. Most of these observations are for rectangular geom-

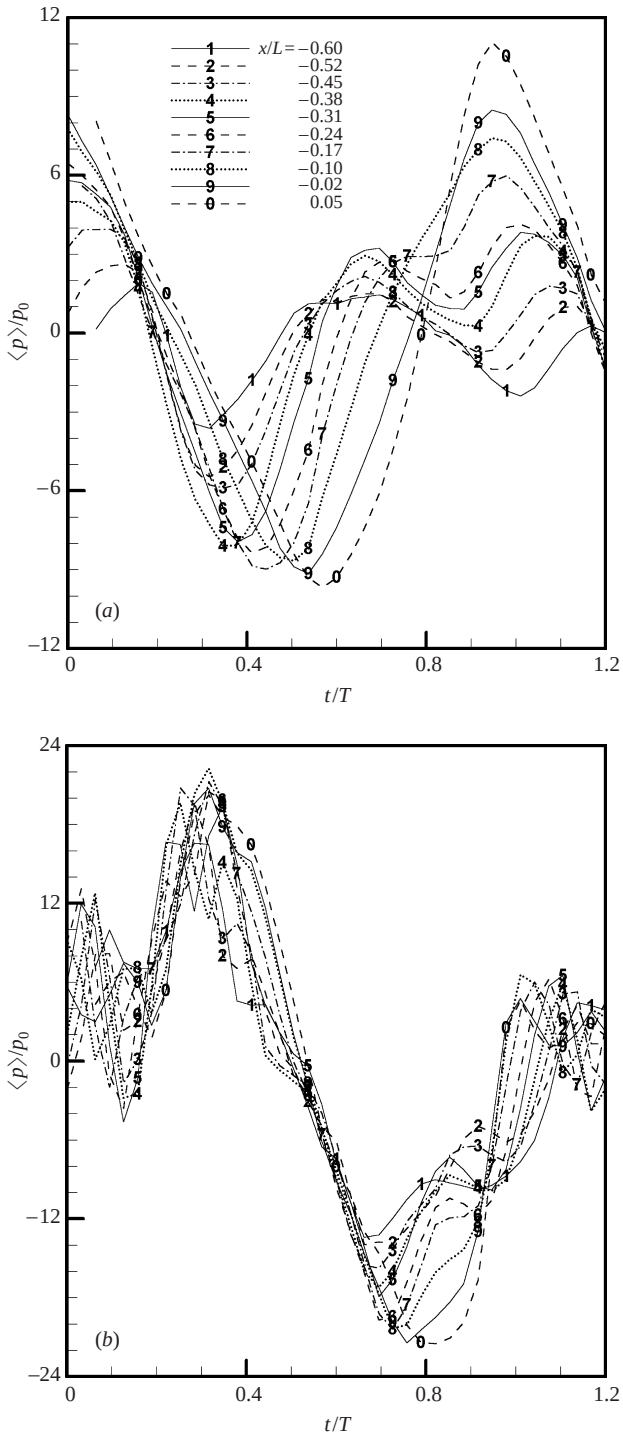


FIGURE 19. Phase-averaged total pressure variations with time at the indicated $x$-locations; time is normalized by the period ($T$) and the ordinate is approximately in percent of plenum pressure ($p_0$). Data are for nozzle 5T1: (*a*) $M_j = 0.55$ ($f_N = 755$ Hz); (*b*) $M_j = 0.75$ ($f_N = 385$ Hz).

etry. Corresponding frequency characteristics are compared with the present results (equation (2)) in § 4.2.

*Bogar, Sajben & Kroutil (1983):* A series of experiments was conducted about twenty years ago for transonic flow through a diffuser by M. Sajben and coworkers (Chen *et al.* 1979; Sajben *et al.* 1980; Bogar *et al.* 1983). They studied a 'low-frequency, self-excited oscillation' occurring in the diffuser. The phenomenon appeared to be the same as the one addressed here. Their flow geometry involved 'one-half' of a two-dimensional diffuser. That is, the floor was flat, the upper wall was convergent–divergent and the two sidewalls were parallel. The throat height ($H$) was 1.73 in. and the 15 in. long diverging section ended with a height of 2.64 in. Following the diverging section there was a parallel section (constant height) of 10 in. length. Experiments were also conducted by extending the parallel section another 28 in. Detailed measurements of unsteady wall pressure with accompanying flow visualization of the unsteady shock were conducted.

They observed multiple spectral peaks in the pressure fluctuation at low supply pressures but a single, strong peak at higher supply pressures. They inferred that the multiple peaks at low supply pressures were longitudinal duct resonance (fundamental and odd harmonics). However, the frequency of the peak at the higher pressure remained invariant for both duct lengths ($L/H = 14.4$ and 30.5), and thus they inferred that it 'did not follow acoustic predictions'. Nevertheless, data for the smaller length (their figure 10) did exhibit an increasing frequency with increasing $M_j$ ($M_j$ inferred from cross-reference to their figure 3). The overall frequency characteristics, including the observation that odd harmonics prevailed at lower pressures, agreed with the present results.

It was not clear why the additional length after the diverging section did not affect the frequency. It is possible that the boundary layer bleed employed just downstream of the diverging section imposed a length scale that remained invariant. Another significant difference is the fact that they had a boundary layer trip at the inlet but the resonance took place nevertheless. Again, there was a boundary layer bleed following the trip. Moreover, the trip was located quite far upstream ($x/H = -6.93$), possibly explaining the 'ineffectiveness' of the trip.

*Hunter 1998:* In this work, steady state results were obtained for the internal flow of a rectangular C–D nozzle (see also Hunter 1993). The nozzle had a throat area of 4.317 in.$^2$, an expansion ratio of 1.797 and a constant width of 3.99 in. While analysing the internal shock structure, the author noted flow unsteadiness at relatively low operating pressures. During a schlieren flow-visualization experiment an audio signal from a microphone was recorded simultaneously with the video records. The author collaborated by performing a preliminary analysis and providing these records. Further analysis of the audio signal revealed spectral peaks very similar to those observed in the present study. This is shown in figure 20. The single peak at $M_j = 0.71$ is apparently due to stage 1 resonance. The frequency increases with increasing $M_j$ and a small peak is detectable at $M_j = 0.96$. At the lowest $M_j$, spectral peaks, apparently for both stages 1 and 2, are present.

The schlieren video records provided by C. A. Hunter allow insight into the unsteady shock motion associated with the resonance. Sample video records for the case of $M_j = 0.71$ are shown in figure 21. The flow is from left to right, and the shock can be seen downstream of the throat. The three pictures are at arbitrary times and chosen to capture the shock at different phases within the oscillation cycle. The shock is complex, with a 'lambda foot', and changes in shape quite drastically within the

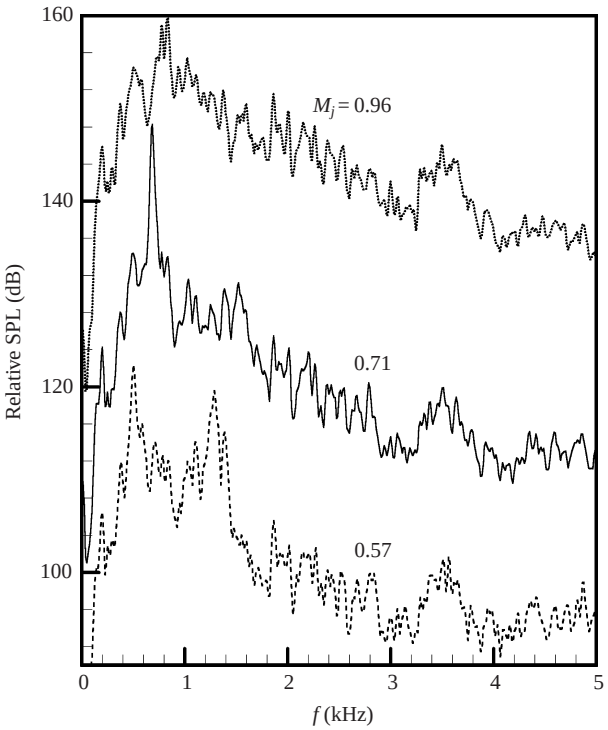


FIGURE 20. Sound pressure spectra from the experiment of C. A. Hunter (1998).

cycle. Corresponding video records at $M_j < 0.57$ (stage 2) indicated a single shock closer to the throat. At $M_j = 0.57$, the shock involved multiple fronts, apparently commensurate with the multiple peaks in the spectra. On the other hand, at $M_j = 0.96$, a clean and well-defined shock with a 'lambda foot' occurred farther downstream. These results aided the discussion of possible mechanism of the phenomenon, in § 5.1.

*Other investigations:* Another past work, that of Meier (1974), merits comment. An unsteady flow oscillation in a two-dimensional C–D nozzle was reported. Vivid flow visualization pictures, showing the shock motion and boundary layer separation, over a cycle of the oscillation were presented. A close look at the results revealed that the boundary layer separation occurred on one wall. This contrasts with the 'symmetric' oscillations noted in the present experiment (§ 3.4). It is not clear if the observed unsteady flow is similar in origin but may suggest that non-symmetrical modes of the transonic resonance are possible.

In connection with research on flow metering by 'venturi nozzles', unsteady quasi-periodic flows were reported in recent publications (Lavante *et al.* 2000; Ishibashi & Takamoto 2001). In particular, the latter work reported axial profiles of 'recovery temperature' inside the divergent section of the nozzle that clearly exhibited standing waves. This is discussed further in § 4.3.

### 4.2. *Frequency scaling for rectangular and co-annular nozzles*

Data from three rectangular configurations have been discussed so far: nozzle 6T1, C. A. Hunter's, and that of Bogar *et al.* (1983). In all three cases the divergence of the nozzle was in one lateral direction while the walls in the other direction were parallel. The frequency characteristics of these as well as the co-annular nozzle (7T1) are now

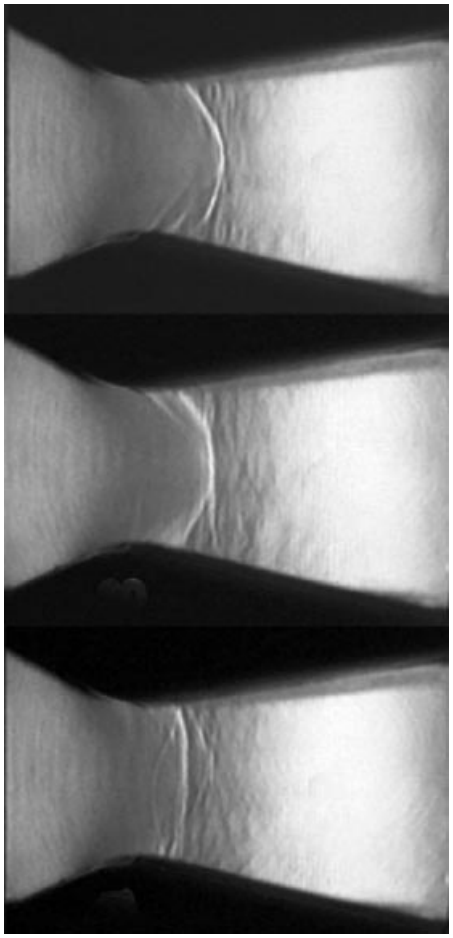


FIGURE 21. Schlieren pictures of the internal shock structure for the $M_j = 0.71$ case of figure 20 (Hunter 1998), for three arbitrary times.

compared with equation (2), referring back to figures 11 and 12. For the comparison, an equivalent half-angle of divergence, $\theta_{eq}$, is defined as follows. With $H_t$ and $H_e$ denoting the heights at the throat and exit, respectively, equivalent diameters $D_{te}$ and $D_{ee}$ are first determined from the areas $(H_t + H_e)^* H_t/2$ and $(H_t + H_e)^* H_e/2$. The value of $\theta_{eq}$ is then obtained similarly to that in the circular case $(= \tan^{-1}(D_{ee} - D_{te})/2L)$. With $\theta_{eq}$ defined this way, the rate of flow divergence with increasing streamwise distance becomes comparable to that for a circular case where the flow diverges circumferentially.

For C. A. Hunter's data (figure 20), the average slope of $fL/a_0$ versus $M_j$ was calculated from the spectral peaks at $M_j = 0.57$ (488 Hz) and $M_j = 0.96$ (825 Hz). The intercept at $M_j = 1$ was obtained by extrapolation. The same procedure was followed to obtain approximate values of these quantities from Bogar *et al.* (1983; from their figures 10 and 3). These results, as well as data for the rectangular and co-annular nozzles of the present experiment, have been shown in figures 11 and 12 by the solid symbols. The index $m = 1$ (equation (2)) yielded the best match. This, together with an inspection of the raw frequency data (no sign of a further frequency jump with increasing $M_j$), indicated that the data for all four cases belonged to stage 1.

The results compared from the two past works are based on quite limited data. Overall, however, it is clear that the slopes (figure 11) and intercepts (figure 12) for all rectangular cases are well represented by equation (2). Data for the co-annular case exhibit some departure. Here, it is possible that the inner flow exerts an influence on the shock structure within the outer annulus. Nevertheless, the departure is small. Thus, equation (2) appears to be applicable to a wide variety of nozzle geometries. It is worth mentioning here that in a recent experiment, transonic tones from even a complex mixer–ejector nozzle could also be successfully predicted by equation (2) (Zaman 2002). Once again, it should be noted that the agreement with equation (2) is achieved only with $\theta_{eq}$ as defined. (If $\theta$ were obtained from equivalent diameters based on the exit and throat areas, the data would scatter. The incompatibility of the latter definition may be appreciated from the fact that $\theta$ would increase with increasing span for a given $L$, and in the limit of infinite span $\theta$ would approach 90°.)

### 4.3. *Numerical simulation*

Key results obtained from a companion numerical study are discussed here. In consideration of an excessive length of the paper, full details of this study have been presented separately (Loh & Zaman 2002).

The simulation was conducted for nozzle 3T2 using the space–time 'conservation element and solution element' (CE/SE) method developed by S.-C. Chang and coinvestigators (Chang, Wang & Chow 1999; Loh, Hultgren & Chang 1998). A modified axisymmetric two-dimensional CE/SE 'inviscid' code was used here. The computational domain started at the inlet of the convergent section and extended over a rectangular subdomain outside the nozzle. The unstructured grid contained about 110 000 triangular cells. The computation was started with the entire flow at rest and with the desired plenum pressure applied at the inlet boundary. A no-slip boundary condition was imposed on the nozzle wall. The calculation was carried out until a 'limit-cycle' oscillation in the flow field was reached. At this state the flow property at a given point in the computational domain would undergo a quasi-periodic oscillation with varying time. Spectrum analysis would exhibit sharp peaks similar to that seen in the experimental data.

The computation was first carried out for $M_j = 0.90$ and the oscillation frequency agreed with the experimental data very well. The fact that an oscillation took place, and that the frequency matched the data so well, prompted further investigation. The computation was performed for four more pressure ratios. The flow oscillation frequencies obtained for these conditions have been compared with the experimental data in figure 3. It can be seen that not only is the trend of increasing frequency with increasing $M_j$ observed, but also the stage jump is captured quite well. For $M_j = 0.90$ (stage 1), numerical schlieren pictures for the internal flow are shown in figure 22. The three phases, approximately equally spaced within the oscillation cycle, were chosen to roughly correspond to the three schlieren pictures of figure 21. Even though the experimental data are for a rectangular geometry while the computation is for an axisymmetric case, the resemblance in the unsteady shock motion is unmistakable.

It is quite clear that the essence of the phenomenon is captured by the computation. Note that it is an 'inviscid' calculation, i.e. viscous terms are set to zero in the governing equations, with a no-slip boundary condition on the wall. Thus, the computed flow involved boundary layer growth due only to 'numerical viscosity'. Boundary layer separation following the shock can be observed in figure 22. However, one may not expect that the details of the separated flow and the separation bubble would be captured faithfully by such a computation. On the other hand, users of the

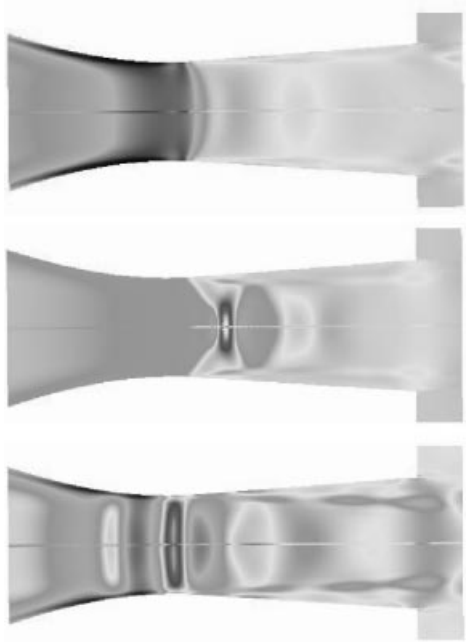

FIGURE 22. Numerical schlieren pictures from the computational study for nozzle 3T2, $M_j = 0.90$ (stage 1).

CE/SE method have demonstrated its ability to capture shock structure relatively faithfully. Thus, one may infer that the exact details of the separated boundary layer are unimportant and it is the shock and its unsteadiness that are critical in the phenomenon under consideration.

The r.m.s. amplitudes of the pressure fluctuation on the centreline are shown in figures 23(*a*) and 23(*b*) for stage 2 and stage 1, respectively. Nodes and antinodes characteristic of standing waves are clearly observed. Here it is instructive to recall the expected standing wave patterns for (no-flow) acoustic resonance of the divergent section (§ 3.2). The fundamental resonance should correspond to a standing one-quarter wave. This would involve a pressure node at the exit and an antinode near the throat. The next 'stage', the third harmonic, should also have a node at the exit and an antinode near the throat; however, there should be an additional pair of a node and an antinode in between. The nodes and antinodes for velocity fluctuation would be the reverse, i.e. a pressure node would correspond to a velocity antinode and vice versa.

It is clear from figure 23 that the resonance in the present case involves standing waves with a similar nodal pattern to that described for the no-flow resonance. Recall from the discussion of figure 19 that aspects of standing waves were noted in the present experiments but the nodal pattern could not be measured with confidence because of probe interference. Referring back to § 4.1, it is noteworthy that in experiments with venturi nozzles Ishibashi & Takamoto (2001) also observed similar standing waves. The time-averaged 'recovery temperature' inside the divergent section of the nozzle, under conditions of unsteady flow, clearly exhibited the presence of one-quarter, three-quarter and even five-quarter standing waves. (In a private communication, Dr Ishibashi confirmed that the flows were accompanied by the emission

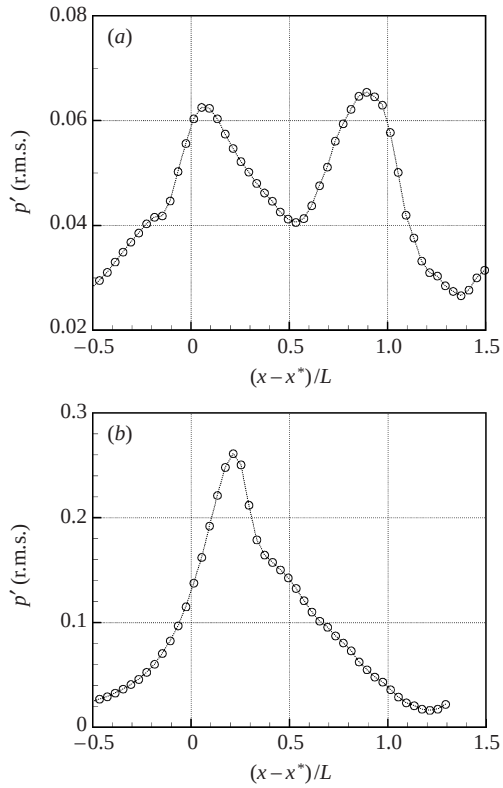


FIGURE 23. Numerical simulation results for pressure fluctuation amplitude (r.m.s.) along the centreline of nozzle 3T2. (*a*) $M_j = 0.60$ (stage 2), (*b*) $M_j = 0.90$ (stage 1).

of tones. Unfortunately, frequencies were not measured that would have allowed a comparison with prediction from equation (2).)

A difference of the present flow with the no-flow acoustic resonance is that the upstream antinode occurs downstream, near the average location of the shock, rather than at the throat. Thus, the resonance here involves the volume of flow from the shock to the nozzle exit. One also finds that the node near the nozzle exit occurs some distance downstream. This is also the case for no-flow resonance, which necessitates a 'length correction' in equation (1). In any case, the presence of the standing waves confirms that the basic mechanism of the transonic resonance must be similar to that of the no-flow acoustic resonance; the physical processes are addressed in the next section.

## 5. Concluding remarks

### 5.1. *Possible mechanism*

A full understanding of the phenomenon and, hence, an analytical formulation for prediction of its characteristics remain incomplete. However, from the accumulated evidence the following may be said:

The phenomenon requires a shock to be present in the diverging section. The shock is followed by boundary layer separation. Farther downstream there is indication of reattachment and, on a time-averaged basis, there appears to be a separation bubble.

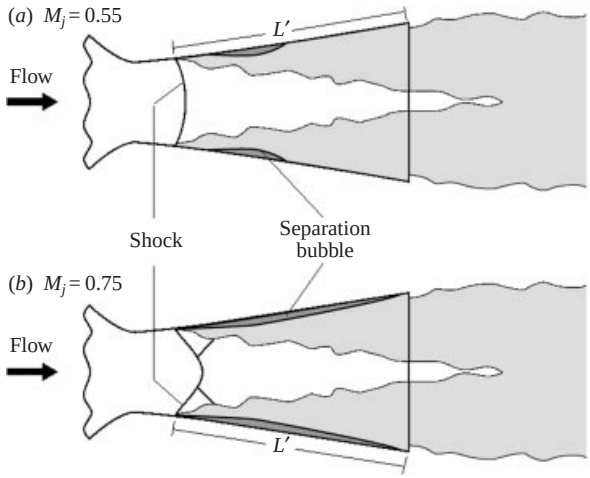


FIGURE 24. Schematic of likely flow fields: (*a*) stage 2; (*b*) stage 1.

Probable flow fields are sketched in figure 24 for the two conditions of figures 17–19. Wall temperature results (figures 14 and 15) together with observations of Bogar *et al.* (1983) and Hunter (1998) aided in constructing these flow fields. A smaller separation bubble is suggested, and a shock occurs just downstream of the throat, at the lower $M_j$. At the higher $M_j$, with the onset of stage 1, it is likely that the shock has developed a 'lambda foot' that would explain the upstream shift of the 'shock location' seen in figures 15 and 16.

The unsteadiness of the shock, apparently stimulated by the unsteadiness of the separated flow, serves as a source of perturbation. Two possibilities may be considered. (i) The separated boundary layer downstream of the shock supports instability wave growth. The downstream-propagating instability (vorticity) wave, upon interaction with the discontinuity at the nozzle exit, produces a feedback wave. This travels upstream at acoustic speed through the subsonic flow and, upon reaching the foot of the shock, completes the feedback loop. In the earlier stage of the investigation (Zaman & Dahl 1999), this was conjectured to be the mechanism. (ii) The mechanism is similar to that involved in longitudinal acoustic resonance. The shock becomes the upstream 'closed' end and also acts like a vibrating diaphragm. Resonance occurs at a frequency when the right impedance condition is satisfied (Morse 1948; see further discussion shortly). An antinode in pressure fluctuation occurs just downstream of the shock while a node occurs near the nozzle exit. The fundamental corresponds to the case when one-quarter wavelength is fitted within the approximate distance from the foot of the shock to the nozzle exit ($L'$).

It is apparent that accumulated evidence points to (ii) as the likely mechanism. The main difficulty with (i) is that it stipulates one full wavelength be contained within the length $L'$ at the fundamental, resonance being possible at all higher harmonics. The results presented in the foregoing indicate that the fundamental in fact corresponds to a one-quarter-wave resonance, commensurate with (ii). Furthermore, even harmonics are absent and resonance at only the odd harmonics takes place.

Certain trends in the data can now be explained qualitatively. Consider a low supply pressure when there is a resonance in stage 2. The shock is somewhere downstream of the throat (figure 24*a*) and a standing '$\frac{3}{4}$-wave' is involved. (The standing waves are not depicted in figure 24 but the reader can imagine a superposition of the

patterns of figure 23 on figure 24.) The distance from the foot of the shock to the exit of the nozzle ($L'$) imposes the length scale while a combination of phase speeds of the downstream- and upstream-propagating waves imposes the time scale. Many of the observations can be reconciled simply by considering the variation of $L'$. As the supply pressure is increased, the shock moves downstream resulting in a decrease in $L'$. This is followed by a decrease in the wavelength and hence an increase in the frequency. With a further increase in supply pressure, a decreasing length $L'$ can no longer support $\frac{3}{4}$-waves and the resonance drops to the $\frac{1}{4}$-wave fundamental. This is accompanied by a decrease in the frequency by approximately a factor of 3. With a further increase in the supply pressure, there is again a decrease in $L'$, resulting in an increase in the frequency. The resonance ceases when the shock location has moved sufficiently downstream when the flow can no longer support the '$\frac{1}{4}$-wave'.

A qualitative explanation can also be given with a similar reasoning for the observed $\theta$-dependence of the frequency curves. Consider that the flow is just choked at the throat at a certain supply pressure. In order to move the shock from the throat to the exit, a finite differential pressure is required for a given divergent section. The required differential pressure to achieve this should be smaller for a smaller value of $\theta$. This can be appreciated by considering the limiting case of $\theta = 0$, when an infinitesimal differential pressure should move the shock from the throat to the exit. Thus, with increasing supply pressure, the rate of decrease in $L'$ is faster when $\theta$ is smaller. This would translate into a steeper slope of the frequency variation with $M_j$, for smaller $\theta$.

It is possible that to a first approximation equation (1) given in § 3.2 might be applicable for prediction of the frequency, after having the length scale $L$ replaced by $L'$. The characteristic dependence of $L'$ on $M_j$ and $\theta$, as discussed in the foregoing, would qualitatively explain the observed frequency variations. The functional dependence of $L'/L$ on $M_j$ and $\theta$, modelled with some simplification and a combination of equations (1) and (2), could be verified against the experimental data.

However, much remains unknown. To appreciate the difficulty, consider first the physical processes in the fundamental acoustic resonance of a cylindrical tube with one end closed and without any flow. The feedback loop involves four segments: (i) a compression wave travels downstream and returns an expansion wave upon exiting the open end, (ii) the expansion wave travels back and is reflected from the closed end, (iii) the reflected expansion wave travels downstream and returns a compression wave upon exiting the open end, (iv) the compression wave travels upstream and is reflected back to complete the cycle. The process yields the 'quarter wave' equation (equation (1) without the square-root term on the right-hand side), with the simplifying fact that the phase-speed is a constant ($a_0$). A similar process is expected in the present flow, with several complications. The phase speeds are likely to be variable with distance as well as with the segment of the feedback loop. The wavefronts may not be 'plane'. We have seen that the shock changes drastically within the cycle. Thus, the location of the upstream reflection boundary for the compression wave may be different from that of the expansion wave. All these factors make it difficult to model the flow with confidence. Thus, further efforts to arrive at a rational set of equations for the prediction of the frequency were not considered at this time.

### 5.2. *Summary*

The main conclusions of the study are enumerated in the following.

1. The subject phenomenon takes place when there is a shock in the diverging section of the nozzle.

2. The frequency variation exhibits a staging behaviour. The fundamental (stage 1) occurs at relatively large supply pressures and corresponds to a standing one-quarter wave. With decreasing pressure, higher stages at only the odd harmonics take place. For all stages, the unsteady fluctuations are found to be of the axisymmetric shape in this experiment.

3. The frequency characteristics are found to depend on the half-angle of divergence of the nozzle, $\theta$. For smaller $\theta$ the slope of the frequency variation with $M_j$ becomes steeper.

4. The distance from the foot of the shock to the exit of the nozzle imposes the length scale, $L'$. The trends in the frequency variation are qualitatively explained simply from the characteristic variation of the length scale $L'$. In a given stage, the shock moves downstream with increasing supply pressure; thus, a decreasing $L'$ leads to an increasing frequency. When $\theta$ is smaller, the shock is pushed downstream at a faster rate with increasing supply pressure; the faster decrease in $L'$ explains the steeper slope of the frequency variation curve.

5. Correlation equations are provided for the prediction of the resonance frequency from a collection of data for single round nozzles. These equations also satisfactorily predict the frequencies for a wide variety of non-axisymmetric nozzles.

6. A companion numerical study captures the essence of the phenomenon. This study suggests that the shock and its unsteadiness govern the resonance, and the exact nature of the separated flow downstream of the shock may not be important in the phenomenon. The numerical results also clearly capture the standing waves at the resonant conditions that were inferred from the experimental data but could not be measured with confidence due to probe interference.

7. The resonance depends on the characteristics of the boundary layer prior to the shock-induced separation. Disturbances placed at locations upstream of the separation tend to suppress the resonance. It is likely that this effect occurs through a disruption of the azimuthal coherence of the unsteady flow. This effect provides an engineering solution for avoiding the resonance as well as reducing 'internal noise' arising from an intermittent occurrence of the resonance. There is a potential for noise benefit simply by suitable tripping of the boundary layer just prior to and aft of the nozzle's throat.

Aerospace Propulsion and Power Research and Technology Base Program supported the work. Thanks are due to Mr John Abbott, Dr Frank Wang, Dr Jayanta Panda of NASA Glenn, Professor Christopher Tam of Florida State University, Mr Craig Hunter of NASA Langley and Professor Ivana Milanovic of the University of Hartford, for inputs in various forms throughout this investigation.

## REFERENCES

Ames Research Staff 1953 Equations, tables and charts for compressible flow. *NACA Rep.* 1135.

Anderson, J. D. 1982 *Modern Compressible Flow with Historical Perspective.* McGraw Hill.

Bogar, T. J., Sajben, M. & Kroutil, J. C. 1983 Characteristic frequencies of transonic diffuser flow oscillations. *AIAA J.* **21**, 1232–1240.

Chang, S.-C., Wang, X.-Y. & Chow, C.-Y. 1999 The space-time conservation element and solution element method: a new high resolution and genuinely multidimensional paradigm for solving conservation laws. *J. Comput. Phys.* **156**, 89–136.

Chen, C. P., Sajben, M. & Kroutil, J. C. 1979 Shock-wave oscillations in a transonic diffuser flow. *AIAA J.* **17**, 1076–1083.

Culick, F. E. C. 1993 Oscillatory and unsteady processes in liquid rocket engines. In *Proc. Combustion Instability in Liquid Rocket Engines* (ed. H. F. R. Schoyer). European Space Agency Rep. WPP-062.

Hill, W. G. & Greene P. R. 1977 Increased turbulent mixing rates obtained by self-excited acoustic oscillations. *Trans. ASME* : *J. Fluids Engng* **99**, 520.

Hsieh, T. & Coakley, T. J. 1987 Downstream boundary effects on frequency of self-excited oscillations in transonic diffuser flows. *AIAA Paper* 87-0161.

Hunter, C. A. 1998 Experimental, theoretical, and computational investigation of separated nozzle flows. *AIAA Paper* 98-3107.

Hunter, C. A. 1993 An experimental analysis of passive shock – boundary layer interaction control for improving the off-design performance of jet exhaust nozzles. MS Thesis, The George Washington University/NASA Langley Research Center.

Hussain, A. K. M. F. & Hasan, M. A. Z. 1983 The 'whistler-nozzle' phenomenon. *J. Fluid Mech.* **134**, 431–458.

Ishibashi, M. & Takamoto, M. 2001 Discharge coefficients of critical nozzles with step near the throat and their flow field estimated from recovery temperature distribution. *2001 ASME Fluids Engineering Division Summer Meeting, New Orleans, LA*. FED SM 2001-18035.

Krothapalli, A. & Hsia, Y. C. 1996 Discrete tones generated by a supersonic jet ejector. *J. Acoust. Soc. Am.* **99**, 777.

von Lavante, E., Zachchial, A., Nath, B. & Dietrich, H. 2000 Numerical and experimental investigation of unsteady effects in critical venturi nozzles. *Flow Meas. Instrum.* **11**, 257–264.

Liu, T., Campbell, B., Burns, S. & Sullivan 1997 Temperature- and Pressure-sensitive luminescent paints in aerodynamics. *Appl. Mech. Rev.* **50**, 227–246.

Loh, C. Y., Hultgren, L. S. & Chang, S.-C. 1998 Computing waves in compressible flow using the space-time conservation element solution element method. *AIAA Paper* 98-0369.

Loh, C. Y. & Zaman, K. B. M. Q. 2002 Numerical investigation of 'transonic resonance' with a convergent-divergent nozzle. *AIAA Paper* 2000-0077.

Mabey, D. G. 1981 Some remarks on buffeting. *Royal Aircraft Establishment, RAE TM Structures* 980, February. (Also Unsteady airloads and aeroelastic problems in separated and transonic flows. *AGARD Conference, Brussels, March 1981*.)

Meier, G. E. A. 1974 Shock induced flow oscillations. *AGARD Proc. Flow Separation*, No. 168.

Morse, P. M. 1948 *Vibration and Sound*. McGraw Hill.

Nakamura, Y. 1968 Some contributions on a control-surface buzz at high subsonic speeds. *J. Aircraft* **5**(2), 118–125.

Powell, A. 1953 On the mechanism of choked jet noise. *Proc. Phys. Soc. Lond.* **66**, 1039–1056.

Raman, G. 1998 Advances in understanding supersonic jet screech: review and perspective. *Progress in aerospace Sciences* **34**, 45–106 (also, *AIAA Paper* 98-0279).

Sajben, M., Bogar, T. J. & Kroutil, J. C. 1980 Unsteady transonic flow in a two-dimensional diffuser. *AFOSR Rep.* TR-80-0628.

Samimy, M., Zaman, K. B. M. Q. & Reeder, M. F. 1993 Effect of tabs at the nozzle lip on the flow and noise field of an axisymmetric jet. *AIAA J.* **31**, 609–619.

Schlichting, H. 1979 *Boundary-Layer Theory*, 7th Edn. McGraw Hill.

Seiner, J. M., NASA Langley Research Center, 1998, private communication.

Tam, C. K. W. 1995 Supersonic jet noise. *Annu. Rev. Fluid Mech.* **27**, 17–43.

Witczak, K. J. 1977 Self-excited oscillations of gas flow in a duct. *Nonlinear Vibration Problems*, 18, pp. 147–207 (Politechnika, Warsaw, Poland), A78-17768.

Zaman K. B. M. Q. 1999 Spreading characteristics and thrust of jets from asymmetric nozzles. *J. Fluid Mech.* **383**, 197–228.

Zaman, K. B. M. Q. 2002 Transonic resonance demonstrated to be a source of internal noise from mixer-ejector nozzles. *Research & Technology 2001, NASA/TM* 2002, 211333, p. 117.

Zaman, K. B. M. Q. & Dahl, M. D. 1990 Some observations on transitory stall in conical diffusers. *AIAA Paper* 90-0048.

Zaman, K. B. M. Q. & Dahl, M. D. 1999 Aeroacoustic resonance with convergent-divergent nozzles. *AIAA Paper* 99-0164.

Zaman, K. B. M. Q., Dahl, M. D. & Bencic, T. J. 2001 Experimental investigation of 'transonic resonance' with convergent-divergent nozzles. *AIAA Paper* 01-0078.

Zaman, K. B. M. Q. & Papamoschou, D. 2000 Study of mixing enhancement observed with a co-annular nozzle configuration. *AIAA Paper* 2000-0094.